

Slow Heating Model of Gamma-Ray Burst: Photon Spectrum and Delayed Emission

KATSUAKI ASANO AND TOSHIO TERASAWA

*Interactive Research Center of Science, Graduate School of Science, Tokyo Institute of
Technology, 2-12-1 Ookayama, Meguro-ku, Tokyo 152-8550, Japan*

asano@phys.titech.ac.jp, terasawa@phys.titech.ac.jp

ABSTRACT

We propose a new mechanism for the prompt emission of gamma-ray burst. In our model electrons are continuously accelerated in the post shock region via plasma turbulence. Using the Monte Carlo technique, we mimic the second-order Fermi acceleration due to plasma turbulence and obtain photon spectra. Since the acceleration balances with the synchrotron cooling, the observed low-energy spectral index is naturally explained. The resultant spectra can be consistent with observed spectra at least below ~ 1 MeV. The model also predicts delayed GeV-TeV emission due to inverse Compton and broad pulse profile of optical emission in some cases. Although nontrivial assumptions are required to reproduce MeV-GeV power-law spectra, the model implies the possibility to explain various kinds of luminosity correlations.

Subject headings: cosmic rays — gamma rays: bursts — gamma rays: theory — radiation mechanisms:

1. Introduction

In the widely discussed internal shock scenario (see, e.g., reviews by Piran 2005; Mészáros 2006), the prompt emission of gamma-ray bursts (GRBs) is due to collisions among inhomogeneities within ultrarelativistic outflows, which lead to formation of shocks. The nonthermal photons, whose typical energy $\varepsilon_p \sim$ a few hundred keV, are emitted from shock-accelerated electrons in highly magnetized plasma. However, several open problems for the internal shock model have been pointed out such as the radiative efficiency, various kinds of luminosity correlations, and so on. In this paper, we focus on the two open problems: the energy transfer problem and the low-energy spectral index problem. The standard

model postulates that a large fraction of the kinetic energy carried by protons should be efficiently converted into that of relativistic electrons. However, it is apparent that the Coulomb interaction cannot transport the internal energy of heated protons into electrons to achieve energy equipartition, because the timescale of the Coulomb interaction is much longer than the dynamical timescale. While the simple first-order Fermi acceleration at the shock front is assumed to transfer the energy into electrons in the standard model, some unknown plasma processes may play an important role in the energy transfer.

The second problem is in the spectral shape of the prompt emission. The observed spectra of GRBs are well fitted with the conventional Band function (Band et al. 1993); the photon number spectrum $\propto \varepsilon^\alpha \exp[-(2 + \alpha)\varepsilon/\varepsilon_p]$ below $(\alpha - \beta)\varepsilon_p/(2 + \alpha)$, and $\propto \varepsilon^\beta$ above it. The typical fitted value of the low energy spectral index is $\alpha = -1.0$ (Preece et al. 2000), while the standard model predicts that photons from cooled electrons dominate the low energy region below ε_p , which leads to $\alpha = -1.5$. To resolve this problem several alternative models, such as the thermal emission from photosphere (Mészáros & Rees 2000; Ioka et al. 2007, and references therein), have been considered. The Klein-Nishina effect on synchrotron self-Compton (SSC) process, which can affect the low energy synchrotron spectrum, has been discussed frequently (Derishev et al. 2001; Bošnjak et al. 2009; Nakar et al. 2009; Wang et al. 2009). Recently, Pe’er & Zhang (2006) have suggested that the decay of magnetic fields (§2) may resolve the problem in the low energy spectral index. However, in that model, we have not yet found a reason why the decay timescale should always be comparable to the cooling timescale (§3). In a particle-in-cell (PIC) simulation for electron-positron plasma (Chang et al. 2008), the decay timescale is close to the requirement of Pe’er & Zhang (2006), but long-term evolution of magnetic fields is still controversial, partially because the effect of accelerated particles is not quantitatively unveiled yet (Keshet et al. 2009).

Motivated by these problems, we propose an alternative model for the prompt emission of GRBs (§4). In our model electron-heating (second-order Fermi acceleration) due to plasma turbulence continues during photon emission in shocked plasmas (Ghisellini & Celotti 1999), so that the resultant spectral index of low energy photons can be consistent with the observations at least below ~ 1 MeV. Since the assumed heating timescale is longer than that in the standard scenario, we call this model the “slow heating model”. After the free energy for the plasma instabilities is dissipated, the magnetic fields may decay and the synchrotron emission will cease. The further possibility to reproduce MeV-GeV power-law spectra within the framework of this model is discussed in §5. In addition, our model naturally predicts delayed GeV-TeV emission due to inverse Compton (IC) and broad pulse profile of optical emission under certain conditions (§6). Finally, we summarize the results of our model, and compare them with the observed luminosity correlations in GRBs (§7). We should

note that our synchrotron model is different from the IC models using the same terminology “slow heating” in Pe’er et al. (2006) and Giannios (2008), in which the electrons are heated slowly in a timescale comparable to the shell-expansion timescale (Ghisellini & Celotti 1999; Stern & Poutanen 2004; Vurm & Poutanen 2009).

2. Magnetic Field: Generation and Decay

In the standard scenario, the magnetic fields are assumed to be generated/amplified in the region around shocks via plasma instabilities, such as the Weibel instability (e.g., Kazimura et al. 1998; Medvedev & Loeb 1999; Silva et al. 2003; Nishikawa et al. 2005; Kato 2007) or the two-stream instability due to high-energy particles accelerated at the shock (e.g., Bell 2004). The difference in temperatures of electrons and protons may also arouse some plasma instabilities. Generated magnetic fields efficiently interact with particles, whose Larmor radii are comparable to the typical scale of the turbulence. This situation is definitely different from the ideal magnetohydrodynamic (MHD) approximation. For example, where the electron Larmor radii are finite, the off-diagonal terms in the electron pressure tensor could appear and catalyze magnetic reconnection (e.g., Mozer and Pritchett 2009). The energy of magnetosonic perturbations can be transferred to resonant particles via the transit-time damping process (e.g., Schlickeiser & Miller 1998). It is natural, therefore, to consider that the generated magnetic fields may decay via interaction with particles after the free energy for instability excitation (anisotropy, inhomogeneity, different temperatures of electrons and ions etc.) is dissipated with a decay timescale t_{dec} . Actually, recent PIC simulations of electron-positron plasmas show that magnetic turbulences induced by the Weibel instability decay (e.g., Chang et al. 2008; Keshet et al. 2009). For $t > t_{\text{dec}}$, electrons stop emitting photons via synchrotron radiation. Therefore, the decay of magnetic fields may suppress the photon emission from cooled electrons, which resolves the problem in the index α .

3. Numerical Model: Standard Case

First let us revisit the effects of decay of magnetic fields with the standard manner of the electron injection. In Figure 1, changing the decay timescale, we show GRB spectra obtained by numerical calculations with the same code in Asano & Inoue (2007, details will be explained in the following section). Throughout this paper, all spectra are shown in terms of the observed fluence versus photon energy, assuming a GRB redshift of $z = 0.1$. The vertical axes denote $\varepsilon f(\varepsilon)$, so that photon spectra with a spectral index α are plotted as

$\propto \varepsilon^{\alpha+2}$. The model parameters are estimated as follows. The emitting region for a pulse is a homogeneous shell expanding with the Lorentz factor Γ at radius R from the central engine. We adopt $l = R/\Gamma$ for the comoving width of the shell, so that the pulse timescale in the observer frame is $\Delta t = R/\Gamma^2 c$ (Sari & Piran 1997). Here, we choose parameters, $\Gamma = 300$, $\Delta t = 0.1$ s, which implies $R = 2.7 \times 10^{14}$ cm. The energy density of accelerated electrons in the shell $U_e = \epsilon_e U$ (U is the total energy density of the shocked plasma) is a parameter that can be directly related to the isotropic-equivalent energy of photons from a single pulse E_{sh} (here we adopt 10^{51} erg) as $E_{\text{sh}} = U_e \mathcal{V}$, where $\mathcal{V} \equiv 4\pi R^3/\Gamma$ is the comoving volume.

In the standard scenario, relativistic electrons are injected at the shock front with a power-law energy distribution $\dot{N}(\gamma_e) \propto \gamma_e^{-p}$ for $\gamma_e \geq \gamma_{e,m}$, where γ_e is the electron Lorentz factor in the plasma rest frame. This scenario requires a sharp low-energy cutoff for the electron injection spectrum; the minimum Lorentz factor $\gamma_{e,m}$ is evaluated in the literature by giving the energy density of electrons $U_e = \epsilon_e U$ together with the total number density of electrons. Therefore, in the standard scenario, $\gamma_{e,m}$ has been conventionally described by the phenomenological parameter ϵ_e , though the energy scale corresponding to $\gamma_{e,m}$ should be derived from physics in relativistic plasmas. Here, instead of ϵ_e , we take $\gamma_{e,m}$ to be a parameter, because we do not concern the non-observable parameter U .

The photon energy ε_p corresponding to $\gamma_{e,m}$ is given by

$$\varepsilon_p \simeq \frac{\hbar e B \gamma_{e,m}^2}{m_e c} \Gamma. \quad (1)$$

The cooling timescale for electrons of $\gamma_{e,m}$ is written as

$$t_c(\gamma_{e,m}) = \frac{6\pi m_e c}{\sigma_T B^2 \gamma_{e,m}}, \quad (2)$$

where σ_T is the Thomson cross section. With a non-dimensional parameter ϵ_B , the magnetic energy density $U_B \equiv B^2/8\pi$ is given as $\epsilon_B U = (\epsilon_B/\epsilon_e)U_e$. In Figure 1, we set $B = 3200$ G and $\gamma_{e,m} = 3900$, which correspond to $\epsilon_B/\epsilon_e = 0.1$ and $\varepsilon_p \sim$ a few hundred keV, respectively.

We numerically follow electron cooling via synchrotron and IC emissions, adopting the Klein-Nishina cross section, and artificially stop the calculation after t_{dec} to mimic the decay of magnetic fields. The effects of $\gamma\gamma$ pair production and synchrotron self-absorption are also taken into account. Since $\gamma_{e,m}\varepsilon_p/\Gamma > m_e c^2$ in our choice, the Klein-Nishina effect cannot be neglected for IC emission. The dynamical timescale $t_{\text{dyn}} = l/c = 30$ s is much longer than the cooling time $t_c = 0.02$ s.

The blue curve with $t_{\text{dec}} = 0.01 t_c \ll t_c$ corresponds to the slow cooling case (Sari et al. 1998). In this case, ε_p is determined by the lowest energy of electrons that can cool within

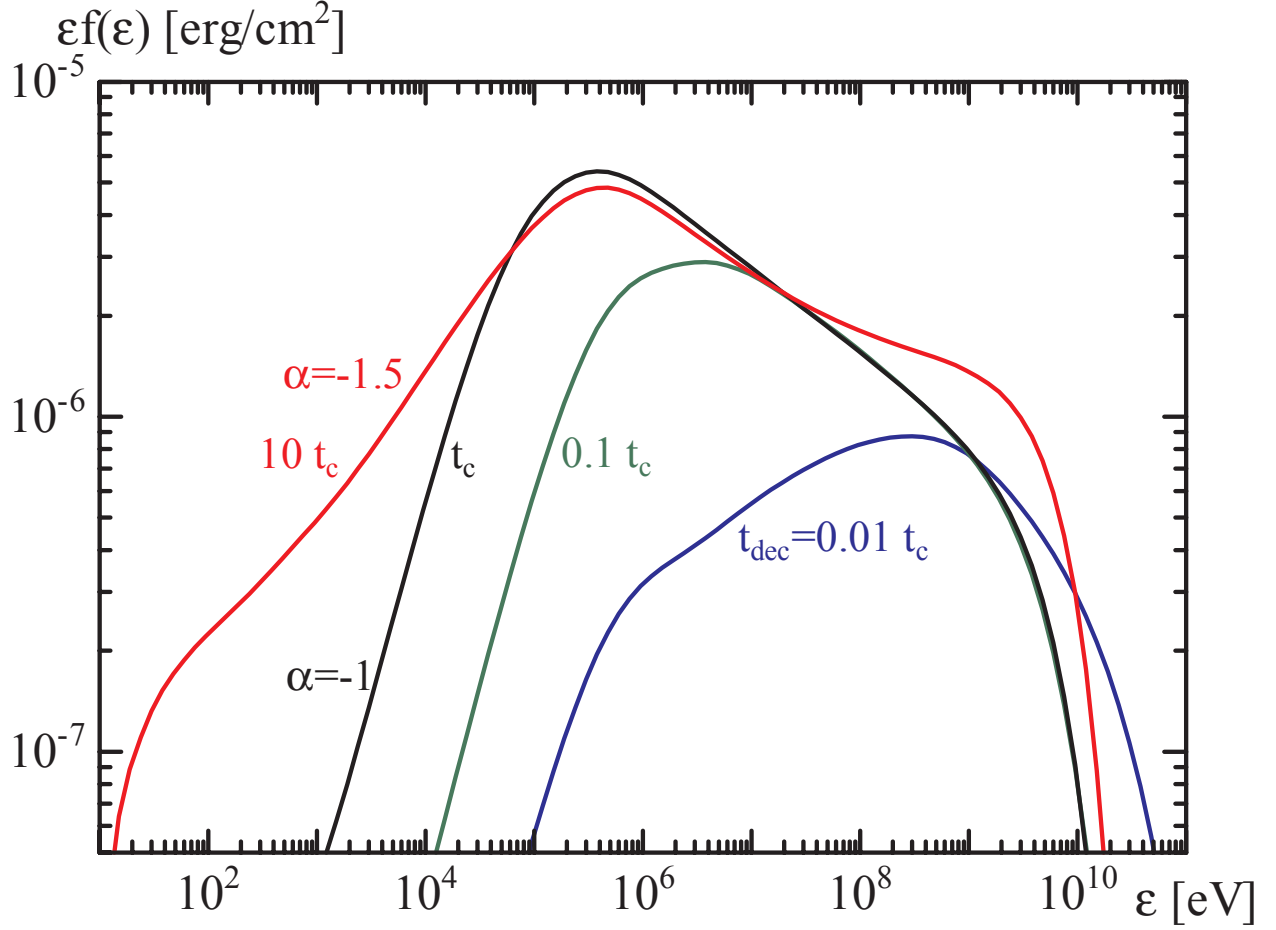


Fig. 1.— Photon spectra for the standard model with decaying magnetic fields varying the decay timescale t_{dec} . The assumed parameters are $p = 2.5$, $E_{\text{sh}} = 10^{51}$ erg, $\Gamma = 300$, $R = 2.7 \times 10^{14}$ cm ($\Delta t = 0.1$ s), $B = 3200$ G, and $\gamma_{e,m} = 3900$.

the timescale t_{dec} . As is well known, the index in the slow cooling case is $\alpha = -(p + 1)/2$, which is softer than the typical observed α for our choice of $p = 2.5$. If we adopt a very hard injection index $p \simeq 1$, α can be ~ -1 , but the high-energy index $\beta = -(p + 2)/2 \sim -1.5$ contradicts the typical value $\beta < -2$. On the other hand, for the two cases, $t_{\text{dec}} = 0.1t_c$ and t_c (green and black curves), the index becomes $\alpha \simeq -1$ below ε_p . These cases are what Pe’er & Zhang (2006) suggested to solve the problem of the low-energy spectral index.

It is further seen in Figure 1 that for the case of $t_{\text{dec}} = 10t_c$ (red curve) the spectrum shows $\alpha \simeq -1.5$. This is the prediction by the standard model as referred in the introduction: electrons injected with $\gamma_e = \gamma_{e,m}$ are cooled after $t = t_c$, and the low-energy spectrum becomes soft owing to emissions from such cooled electrons. It is noted that this case shows a spectral

bump in the GeV band due to IC emission, whose contribution is boosted up by enhancement of low-energy seed photons. We can also see cutoffs above 10 GeV and below 30 eV. They are $\gamma\gamma$ -absorption and synchrotron self-absorption, respectively.

The above results indicate that only with the case, $t_{\text{dec}} \sim t_c(\gamma_{e,m})$, the decaying magnetic field can explain the low-energy index α . However, there is no definite physical reason to expect such a matching between t_{dec} and $t_c(\gamma_{e,m})$. The jitter radiation (Medvedev 2000; Fleishman 2006) instead of the synchrotron radiation is worthwhile to consider, because the typical scale of turbulence excited by plasma instabilities can be much shorter than the Larmor radii of radiating electrons. While the typical photon energy in the jitter radiation, which is determined by the coherence scale of the disturbed magnetic field, differs from in the usual synchrotron radiation, the introduction of the jitter radiation does not significantly change the low-energy spectral shape: α remains $\simeq -1.5$ as long as $t_{\text{dec}} \gg t_c$ (fast cooling).

4. Slow Heating Model: start

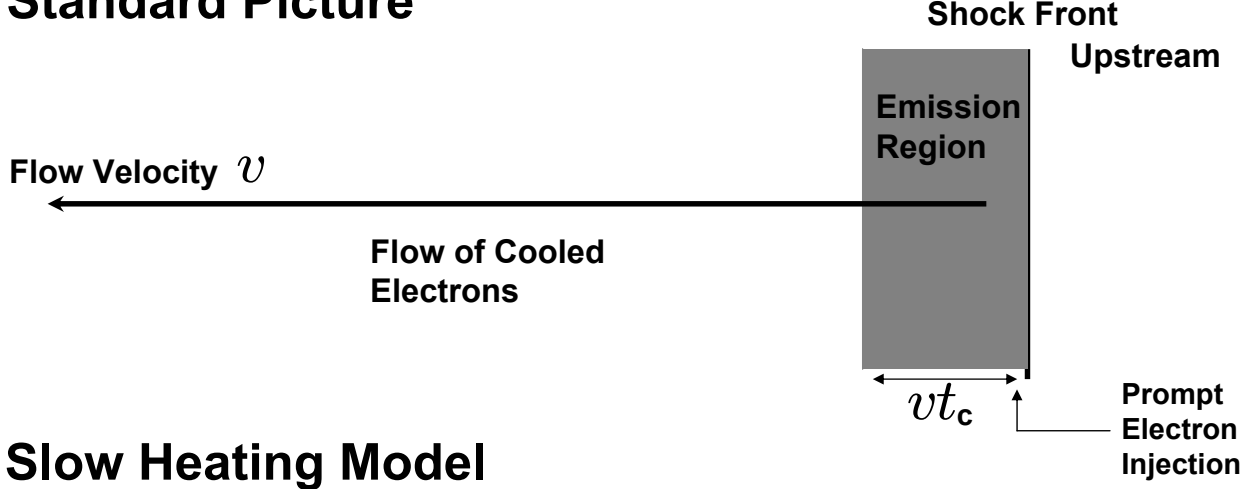
As we mentioned in §2, turbulent magnetic fields may be generated in the plasmas around shocks. Such turbulent waves may play a role in energy transfer from protons to electrons until the magnetic fields decay. In this section we present our new model, the slow heating model, to resolve the index problem. While the standard picture postulates a prompt acceleration of electrons, whose timescale is much shorter than $t_c(\gamma_{e,m})$, our model assumes slower energy transfer from the background plasma to electrons via some unknown plasma instabilities (see Figure 2).

In order to mimic the energy transfer we consider the second-order Fermi acceleration, even though there may exist not only Alfvén waves but also other types of acceleration mechanisms such as electric fields around ion current channels (Heddal et al. 2004) or coherent wave-particle interactions resulting from parametric instabilities (Matsukiyo & Hada 2009), which can also contribute to particle acceleration. When a particle is scattered by a wave or magnetized cloud preserving its energy in the wave (cloud) frame, twice Lorentz transformations give us energy gain due to this collision $\xi \equiv \Delta E/E$ as

$$\xi = \gamma_0^2 (1 - \beta_0 \mu_1 + \beta_0 \mu'_2 - \beta_0^2 \mu_1 \mu'_2) - 1, \quad (3)$$

where $\gamma_0 = 1/\sqrt{1 - \beta_0^2}$, μ_1 , and μ'_2 are the Lorentz factor of the wave (cloud), cosines of incident angle in the reference frame, and scattering angle in the wave (cloud) frame, respectively. If the wave velocity is non-relativistic ($\beta_0 \ll 1$), the mean energy gain $\bar{\xi} \sim \beta_0^2$ under the assumption of isotropic wave distribution $\overline{\mu_1} = -\beta_0/2$ and isotropic scattering $\overline{\mu'_2} = 0$. So the second-order Fermi acceleration is a slower acceleration process than the

Standard Picture



Slow Heating Model

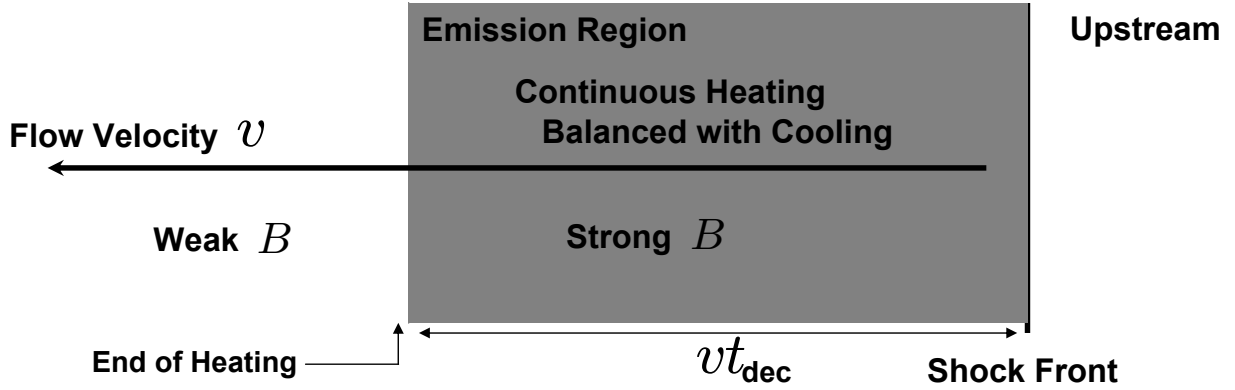


Fig. 2.— Schematic pictures of the standard model and slow heating model. In the standard picture, radiation from the area behind the emission region cannot be neglected, as long as the magnetic field remains. On the other hand, the end of heating due to plasma turbulence and decay of the magnetic field are naturally simultaneous in the slow heating model.

first-order one ($\bar{\xi} \sim \beta_0$) in non-relativistic cases. However, GRB internal shock is relativistic so that we can expect turbulent magnetic fields with $\beta_0 \sim 1$.

The Fokker-Planck equation for ultrarelativistic particles can be written as

$$\frac{\partial N}{\partial t} = \frac{\partial}{\partial E} D_{EE} \frac{\partial N}{\partial E} - \frac{\partial}{\partial E} \left[\left(2 \frac{D_{EE}}{E} - \dot{E}_{cool} \right) N \right], \quad (4)$$

where D_{EE} is the energy diffusion coefficient (see, e.g., Liu et al. 2006). Defining the mean free time of particles t_{coll} , we can write

$$D_{EE} = \frac{\bar{\xi} E^2}{2t_{coll}}, \quad (5)$$

and the acceleration timescale $t_{\text{acc}} = t_{\text{coll}}/\bar{\xi}$. At present we have no reliable model of relativistic turbulence in GRBs. For reference, let us look in stochastic acceleration in non-relativistic plasma. When we express the diffusion coefficient as $D_{EE} \propto E^n$ ($t_{\text{acc}} \propto E^{2-n}$), we obtain $n = m$ for isotropic Alfvén turbulence of spectral energy density per unit wavenumber $W_k \propto k^{-m}$ (see, e.g., Miller & Ramaty 1989). The model with $n = 2$ is often adopted for small scale MHD turbulences (see, e.g., Liu et al. 2006). Another value $n = 5/3$ is frequently used for the Kolmogorov turbulence. The strong turbulence limit (Bohm limit), where the mean free path becomes comparable to Larmor radii, corresponds to the case of $n = 1$, where the dependence on m disappears. Relativistic shocks in electron-positron plasmas in PIC simulations (Chang et al. 2008) generate magnetic turbulence with $m = 0$ for small k ($kc \ll$ plasma frequency), but $m \simeq 2$ for large k . Although we have no definite shape of D_{EE} for GRBs yet, future long-term PIC simulations may reveal the property and evolution of magnetic turbulence.

From eq. (4) we may write $\overline{\Delta E^2} = (\bar{\xi} - \bar{\xi}^2)E^2$, so that we assume the probability function of ξ per collision as a Gaussian form,

$$P(\xi) = \frac{1}{\sqrt{2\pi}\sigma} \exp\left[-\frac{(\xi - \bar{\xi})^2}{2\sigma^2}\right], \quad \sigma = \sqrt{\bar{\xi} - \bar{\xi}^2}. \quad (6)$$

Hereafter, we assume a constant value of $\bar{\xi} = 0.1$. Considering synchrotron and IC emissions, the energy loss rate due to radiative cooling is expressed as

$$\dot{E}_{\text{cool}} = \frac{4}{3}\sigma_{\text{T}}c\gamma_e^2 U_B \left(1 + K(\gamma_e)\frac{U_{\text{ph}}}{U_B}\right), \quad (7)$$

where U_{ph} and $K(\gamma_e)$ are the photon energy density and the correction coefficient due to the Klein-Nishina effect, respectively. In the Thomson limit, $K(\gamma_e) = 1$.

We employ the Monte Carlo numerical code of Asano & Inoue (2007) to follow the radiative cooling and stochastic energy gain/loss processes according to eqs. (7) and (6) with a time step,

$$\delta t = \min(t_{\text{coll}}/30, E/\dot{E}_{\text{cool}}/30, t_{\text{dec}}/30), \quad (8)$$

and at $t = t_{\text{dec}}$, we artificially halt the calculations to mimic the decay of magnetic fields. For each time step, we judge the occurrence of collision and estimate energy loss due to radiation using random numbers. If a collision occurs, the energy gain/loss due to the collision is counted with evaluated ξ .

Since highly disturbed magnetic fields are assumed, it is meaningful to consider the jitter radiation (Medvedev 2000; Fleishman 2006). But, for simplicity, we consider usual

synchrotron radiation, using the synchrotron function (Rybicki and Lightman 1979). As for IC emission we numerically estimate the spectral photon emission rate and $K(\gamma_e)$ by integrating the photon energy distribution given in advance with the Klein-Nishina cross section σ_{KN} (Rybicki and Lightman 1979). We assume a uniform and isotropic photon field within a shell with width $l = R/\Gamma$ in the shell frame. To obtain photon spectra, the energy distributions of photons and particles are simulated iteratively until the resultant spectrum and presupposed spectrum are identical.

In addition we take into account $\gamma\gamma$ pair production and synchrotron self-absorption. However, these processes are not so important in this paper, so that we omit the explanation of the method to include these effects (see Asano & Inoue 2007).

The studies for plasma turbulences in the post shock region by many authors are ongoing now. Although remarkable development is seen in recent PIC simulations and MHD simulations (e.g., Zhang et al. 2009), a definite picture of shocked plasma is not understood yet. Here, we consider a simple toy model assuming that $D_{EE} \propto E^2$, which means that t_{coll} does not depend on the energy of electrons. Although we take into account IC emission, it is not a main subject to discuss in this paper. In order to concentrate on synchrotron photon spectra, we adopt a stronger magnetic field $B = 10^4$ G. The other parameters are the same as those in §3 except for the electron injection. The typical photon energy is expected to be emitted from electrons, whose energy loss rate is balanced with the second-order Fermi acceleration. Therefore, we adjust t_{coll} to make $t_{\text{acc}} = t_c$ at $\gamma_e = \gamma_{\text{typ}} = 3100$ ($t_c(\gamma_{\text{typ}}) \equiv t_{c,\text{typ}} \sim 2 \times 10^{-3}$ s) that implies the typical photon energy $\varepsilon_p(\gamma_{\text{typ}}) \sim$ a few hundred keV. The Klein-Nishina effect is important for electrons of $\gamma_e = \gamma_{\text{typ}}$ even in this case. The number of electrons is roughly adjusted to make $E_{\text{sh}} = 10^{50}\text{-}10^{51}$ erg considering the heating rate and t_{dec} (we may not exactly forecast the final photon energy in advance). Below (above) γ_{typ} the acceleration timescale is shorter (longer) than the synchrotron cooling timescale. The heating due to turbulence reduces the effective number of electrons below γ_{typ} so that the low-energy photon spectrum is expected to be harder than the standard one (the red line in Figure 1) even for $t_{\text{dec}} \gg t_{c,\text{typ}}$. At $t = 0$ electrons are injected with monochromatic energy of $\gamma_e = \gamma_{\text{inj}} = \gamma_{\text{typ}}/10$. We have confirmed that a run with 5000 particle histories is enough to converge. In order to verify that the low-energy photon spectra become hard enough ($\alpha \sim -1$) even for a longer decay timescale than the cooling timescale, we adopt $t_{\text{dec}} = 30t_{c,\text{typ}}$. The result is shown in Figure 3.

Photons at the spectral peak are emitted from electrons of $\gamma_e \sim \gamma_{\text{typ}}$ as anticipated in advance. Since electrons are accelerated immediately, the injection parameter γ_{inj} does not affect the resultant spectrum very much. The low-energy spectral index is well approximated as ~ -1 . The spectral bump at \sim GeV is due to IC emission, whose contribution is small

because of high B ($\epsilon_B/\epsilon_e \sim 3$) and Klein-Nishina effect. Compared to Figure 1, the lower density of target photons (≥ 2 MeV) weakens the $\gamma\gamma$ absorption effect on IC emission. The overall shape of the spectrum is different from the Band function. We magnify the spectrum for 10 keV–1 MeV range in Figure 3(b). In this energy range, the spectrum with artificial errors (10%) does not contradict the Band function very much, even though the model is quite simple.

5. Slow Heating Model: modification

While the model spectra in §4 may be fitted with the Band function below \sim MeV, some GRBs show power-law spectra in the MeV-GeV range with $\beta \sim -2$ (see Abdo et al. 2009a, as one of the recent examples). As numerous simulations for the broadband prompt emission spectrum have shown (e.g., Pe’er et al. 2006; Gupta & Zhang 2007; Asano & Inoue 2007; Bošnjak et al. 2009), the usual simple power-law injection for electrons can easily reproduce the MeV-GeV power-law spectra. In the slow heating model, one of the simplest interpretation to overcome this difficulty is that such power-law spectra are superpositions of multiple components with different ϵ_p . This explanation requires fine adjust of the amplitude of multiple components. Although this interpretation remains viable so far, we search for alternative ideas within the slow heating model in this section.

In §4, the index n of energy dependence of $D_{EE}(\propto E^n)$ was taken 2. To make the resultant energy spectrum harder, we first test the cases with $n > 2$ (note that $t_{\text{acc}} < t_c$ for $n > 3$ in higher energy range). Our simulations show that the spectral shape becomes close to a power-law function as n increases. However, even for an extreme choice of $n = 3$ ($t_{\text{acc}} \propto E^{-1}$), the resultant index $\beta = -3.2$ is still not hard enough.

Since we consider the decay of the magnetic fields, it is natural to let $D_{EE} = 2\bar{\xi}E^2/2t_{\text{coll}}$ also time (or equivalently distance from the shock front) dependent. Our toy model assumes a power-law shape as $t_{\text{coll}} \propto \gamma_e^0 t^x$ with upper and lower limits. Namely,

$$t_{\text{coll}} = \min \left[\bar{\xi}t_{c,\text{typ}}, \max \left\{ t_{\text{min}} \left(\frac{t}{t_{\text{min}}} \right)^x, t_{\text{min}} \right\} \right], \quad (9)$$

where $t_{\text{min}} \equiv \bar{\xi}t_{c,\text{typ}}/100$ in our model. In this case, the initial short timescale of acceleration makes ϵ_p higher, and as the acceleration timescale elongates with time, ϵ_p will be settled around a few hundred keV. Here, to harden spectra, we adopt $\gamma_{\text{inj}} = 10\gamma_{\text{typ}}$. Since the acceleration time from γ_{inj} to $100\gamma_{\text{typ}}$ is $\sim 10t_{\text{min}} \gg t_{\text{min}}$, the highest photon energy may be ~ 100 MeV emitted from electrons of $\gamma_e = \gamma_{\text{inj}}$ (10 GeV photons from electrons of $\gamma_e = 100\gamma_{\text{typ}}$ may not be produced so much). Assuming $t_{\text{dec}} = 300t_{c,\text{typ}}$ (other parameters are the same as before), we calculate spectra (see Figure 4).

We can see that the spectra above ε_p for $\chi = 0.3$ and 0.4 are well approximated by power-law functions. Even for $\chi = 0.5$, the spectrum from ~ 500 keV to ~ 3 MeV can be accepted as a power-law function. The peak energy ε_p for $\chi = 0.3$ becomes above MeV, because t_{acc} at $t = t_{\text{dec}}$ is still shorter than the final acceleration timescale assumed in advance, $\bar{\xi}t_{c,\text{typ}}$. For $\chi = 0.5$, after $t = 10t_{c,\text{typ}} \ll t_{\text{dec}} = 300t_{c,\text{typ}}$, the timescale t_{coll} attains the upper limit $\bar{\xi}t_{c,\text{typ}}$, which makes $\gamma_e \sim \gamma_{\text{typ}}$. Compared to the timescale of stay around γ_{inj} , the longer stayover around γ_{typ} yields the spectrum bump around a few hundred keV as set in advance. So one may easily understand that the spectra in this model depend on the timescale t_{dec} . Figure 5 shows that the spectral bump around ε_p grows as t_{dec} extends. It is apparent that the upper limit for t_{coll} , whom we set up to adjust ε_p , causes the bumps. If t_{coll} is elongated monotonically, ε_p is determined by t_{coll} at $t = t_{\text{dec}}$ as the case of $\chi = 0.3$ in Figure 4.

The models of D_{EE} in this section are toy models to demonstrate the capability of MeV-GeV power-law spectrum in the slow heating model. In addition, we have assumed the monochromatic injection of electrons. The actual plasma turbulence and electron injection mechanism may be more complicated than the models we tested. The strength of magnetic fields may evolve with D_{EE} , or the first-order Fermi acceleration or surfing/drift/wake-field acceleration (see, e.g., Amano & Hoshino 2007; Hoshino 2008) may work as the injection mechanism at shock front. Although we need the nontrivial shape of D_{EE} to reproduce the high-energy power-law spectra, the actual GRB plasmas may provide favorable conditions for MeV-GeV emissions. PIC simulations can be strong tools to verify this scenario. For example, Chang et al. (2008) show that the energy density of magnetic turbulence in electron-positron plasma evolves as $\propto t^{-2/3}$ initially, then steepens to $\propto t^{-1}$ later. Such results encourage the model we discussed in this section.

6. Delayed Emission

In the simulations discussed in the previous sections, we have artificially halted the calculations at $t = t_{\text{dec}}$ with constant magnetic fields. However, the actual magnetic fields may not disappear suddenly, and we may expect residual magnetic fields at $t > t_{\text{dec}}$. In this section, we consider emissions after the decay of magnetic fields. Here, we assume a simple exponential decay and residual magnetic fields as

$$B = \max(B_0 e^{-t/t_{\text{dec}}}, B_{\text{min}}), \quad (10)$$

where B_0 and B_{\min} are constants. As for the acceleration timescale, to get rid of the heating effect smoothly, we assume the rapid evolution of t_{coll} as

$$t_{\text{coll}} = \min \left(\bar{\xi} t_{c,\text{typ}} e^{(t/t_{\text{dec}})^2}, t_{\text{dyn}} \right). \quad (11)$$

We numerically follow electron cooling/heating and photon emission during a period of $t_{\text{sim}} = t_{\text{dyn}} = l/c \gg t_{\text{dec}}$ with $\gamma_{\text{inj}} = \gamma_{\text{typ}}/10$ and $t_{\text{dec}} = 30t_{c,\text{typ}}$ (see Figure 6). Two parameter sets are adopted; one is the same as that in §4 ($\Gamma = 300$, $\gamma_{\text{typ}} = 3100$, $R = 2.7 \times 10^{14}$ cm, $B_0 = 10^4$ G), and another parameter set describes a higher Γ case with the same ε_p and Δt : $\Gamma = 800$, $\gamma_{\text{typ}} = 7800$, $R = 1.9 \times 10^{15}$ cm, and $B_0 = 530$ G. For the final magnetic fields, $B_{\min} = 1$ G is adopted in both the two cases, though there is no clue to the residual magnetic fields at present. For $t \ll t_{\text{dec}}$, the photon emission mechanism is the same as those in §4. However, after $t = t_{\text{dec}}$, the main cooling mechanism is switched from synchrotron to IC, because the photon density is assumed to be constant within the shell of width l .

Comparing the thin dotted line with solid lines in Figure 6, it is clearly shown that the residual energy of electrons at $t = t_{\text{dec}}$ is emitted via IC emission in GeV-TeV ranges. The typical photon energy due to IC largely depends on Γ . As shown by the long dashed line in Figure 6, $\gamma\gamma$ absorption affects the final spectrum for $\Gamma = 300$ above 10 GeV (close to the cases of Figure 1), while it is negligible for $\Gamma = 800$ owing to the lower photon density. Therefore, this case indicates a delayed onset of GeV-TeV photons compared to MeV photons with a timescale of $\sim t_{\text{dec}}/\Gamma$. On the other hand, the spectral shape in the low-energy region is not altered in this model as seen in Figure 6.

Recent GRBs detected by *Fermi*-LAT tend to show such a delayed onset of high-energy (> 100 MeV) emission (GRB 080916C, GRB 080825C, etc.; Abdo et al. 2009a,b). However, it is noted that the broadband spectral shape for GRB 080916C is not well reproduced by our simple toy model. Future observations with *Fermi* or Cerenkov telescopes will testify the model prospects and yield a clue to the refinement of the model.

Next, let us consider photon emission in longer timescales than the dynamical timescale t_{dyn} . In the standard scenario, emission after the dynamical timescale may be negligible because of the fast cooling of electrons. However, in our scenario, the residual electron energy may be released via synchrotron radiation, which can contribute to optical emissions as seen in some GRBs (Vestrand et al. 2005; Blake et al. 2005). Our results for such cases are shown in Figure 7, where the parameters are the same as those for $\Gamma = 300$ in Figure 6, but $t_{\text{sim}} = 10t_{\text{dyn}}$, $B_{\min} = 1, 10$ and 30 G, and rapid decay of the photon density $\propto \exp[-(t/t_{\text{dec}})^2]$. For simplicity, we neglect the effects of adiabatic cooling due to shell expansion.

As seen in Figure 7, optical synchrotron emissions become more luminous than the flu-

ence of the power-law extrapolation from the X-ray spectra. Most of the optical photons are emitted after $t = t_{\text{dyn}}$ in the weak magnetic fields so that broader pulse profile is expected for optical than γ /X-ray bands. Such longer variability timescales in prompt optical emission is seen in GRB 080319B (Racusin et al. 2008), though the flux is brighter than the extrapolation from the X-ray spectra by 3-4 orders of magnitude (1-2 orders in our results). More luminous optical emissions as compared to X-ray may be possible, if we change t_{dec} . Since our objective in this paper is not to reproduce spectra of specific GRBs, we do not further discuss the fraction of optical flux here.

7. Summary and Discussion

Motivated by the energy transfer and low-energy spectrum problems, we propose a new model to reproduce GRB prompt emissions. In this model, electrons are continuously heated via plasma turbulences within a timescale longer than the cooling timescale. The acceleration timescale is assumed to be much longer than that in the standard picture. Emissions from cooled electrons are suppressed so that the low-energy spectral index α is close to the observed value -1 . At least below MeV, the model spectrum does not contradict the Band function very much. Considering that most of the GRB spectra were obtained in energy ranges below MeV, the model spectra may be consistent with a large fraction of GRBs. In order to explain power-law spectra in MeV-GeV range observed in some GRBs, we need a superposition of multiple components with different ε_p , or nontrivial shape and evolution of the diffusion coefficient. Our model, under certain conditions, predicts delayed GeV-TeV emission via IC or delayed optical emission with broad pulse profile via synchrotron. We expect that the accumulation of many GRB observations will verify the characteristics predicted by our model in near future.

Roughly speaking, the energy release in this model is estimated as $\Gamma N(t_{\text{dec}}/t_{c,\text{typ}})\gamma_{\text{typ}}m_e c^2$, where N is the total number of accelerated electrons. Given the total isotropic energy $E_{\text{iso}} = 4\pi R^3 U$, the required number of electrons depends on t_{dec} . Thus, the fraction of accelerated electrons can be much less than unity in this model, while many authors have frequently assumed that all electrons are accelerated (see Eichler & Waxman 2005).

One interesting point in our model is that the physical explanation for the spectral peak energy ε_p is clear. The balance between synchrotron cooling and heating provides us the typical electron energy $\gamma_{\text{typ}}m_e c^2$, from which we can estimate ε_p . The spectral peak and low-energy index are reproduced by this mechanism unless $t_{\text{acc}} \gg t_c$. One remaining problem is why shocked plasma in GRBs always adjust t_{coll} to make ε_p observed range of ~ 1 MeV. To explain this we need another assumption; for example, $D_{\text{EE}} \propto U_B$, which implies $t_{\text{acc}} \propto B^{-2}$.

The balance between cooling time $t_c \propto B^{-2}$ and t_{acc} gives us $\gamma_{\text{typ}} \propto B^0$. Since we may write the luminosity as $L_{\text{iso}} = E_{\text{iso}}/(R/c\Gamma^2) = 4\pi(\epsilon_e/\epsilon_B)U_B R^2 \Gamma^2$, we obtain

$$\varepsilon_p \propto \Gamma B \gamma_{\text{typ}}^2 \propto (\epsilon_e/\epsilon_B)^{-1/2} L_{\text{iso}}^{1/2} R^{-1}, \quad (12)$$

where Γ -dependence disappears. These results are consistent with the Yonetoku relation ($\varepsilon_p \propto L_{\text{iso}}^{0.5}$; Yonetoku et al. 2004), except for the factor R^{-1} . Of course, the above assumption is not trivial. When we assume $D_{EE} \propto U_B^x$, the correlation becomes $\varepsilon_p \propto L_{\text{iso}}^{(3-2x)/2} \Gamma^{2x-2} R^{2x-3}$. If the jitter radiation is applicable, in which the typical photon energy depends on the coherent scale of the field, the Yonetoku relation implies some correlations between the typical scale of turbulence and luminosity. In any case, fundamental studies of the long-term evolution of relativistic plasmas, based on PIC simulations, etc., are indispensable to verify the model and luminosity correlations.

For the *Fermi*-LAT GRB 080916C, by a process of elimination, Zhang & Pe'er (2009) conclude that this GRB is emitted from a magnetically dominated outflow. In such a case, the dissipation of the bulk kinetic energy may not be due to internal shocks, because the Alfvén velocity is very close to the light speed. In order to produce non-thermal particles, the dissipation of magnetic fields such as magnetic reconnection, etc. should occur in the outflow. The dissipation processes of magnetic fields may generate magnetic turbulences so that we can expect the second-order Fermi acceleration in this case too.

We appreciate the anonymous referee for the useful advice. This work is partially supported by the Grant-in-Aid for Scientific Research, No. 21540259 from the MEXT of Japan.

REFERENCES

- Abdo, A. A. et al. 2009a, *Science*, 323, 1688
 Abdo, A. A. et al. 2009b, *ApJ*, submitted
 Amano, T., & Hoshino, M. 2007, *ApJ*, 661, 190
 Asano, K., & Inoue, S. 2007, *ApJ*, 671, 645
 Band, D. et al. 1993, *ApJ*, 413, 281
 Bell, A. R. 2004, *MNRAS*, 353, 550
 Blake, C. H. et al. 2005, *Nature*, 435, 181

- Bošnjak, Ž., Daigne, F., & Dubus, G. 2009, *A&A*, 498, 677
- Chang, P, Spitkovsky, A., & Arons, J. 2008, *ApJ*, 674, 378
- Derishev, E. V., Kocharovsky, V. V., & Kocharovsky, VI. V. 2001, *A&A*, 372, 1071
- Eichler, D., & Waxman, E. 2005, *ApJ*, 627, 861
- Fleishman, G. D. 2006, *ApJ*, 638, 348
- Ghisellini, G., & Celotti, A. 1999, *ApJ*, 511, L93
- Giannios, D. 2008, *A&A*, 480, 305
- Gupta, N., & Zhang, B., 2007, *MNRAS*, 380, 78
- Hededal, C. B., Haugbølle, T., Frederiksen, J. T., & Nordlund, Å. 2004, *ApJ*, 617, L107
- Hoshino, M. 2008, *ApJ*, 672, 940
- Ioka, K., Murase, K., Toma, K., Nagataki, S., & Nakamura, T. 2007, *ApJ*, 670, L77
- Kazimura, Y., Sakai, J. I., Neubert, T. & Nulanov, S. V. 1998, *ApJ*, 498, L183
- Kato, T. N. 2007, *ApJ*, 668, 974
- Keshet, U., Katz, B., Spitkovsky, A., & Waxman, E. 2009, *ApJ*, 693, L127
- Liu, S., Melia, F., Petrosian, V., & Fatuzzo, M. 2006, *ApJ*, 647, 1099
- Matsukiyo, S., & Hada, T. 2009, *ApJ*, 692, 1004
- Medvedev, M. V. 2000, *ApJ*, 540, 704
- Medvedev, M. V., & Loeb, A. 1999, *ApJ*, 526, 697
- Mészáros, P. 2006, *Rep. Prog. Phys.*, 69, 2259
- Mészáros, P., & Rees, M. J. 2000, *ApJ*, 530, 292
- Miller, J. A., & Ramaty, R. 1989, *ApJ*, 344, 973
- Mozer, F. S., & Pritchett, P. L. 2009, *Geophys. Res. Lett.*, 36, L07102
- Nakar, E., Ando, S., & Sari, R. 2009, *ApJ*, 703, 675
- Nishikawa, K.-I. et al. 2005, *ApJ*, 622, 927

- Pe'er, A., Mészáros, P. & Rees, M. J. 2006, *ApJ*, 642, 995
- Pe'er, A., & Zhang, B. 2006, *ApJ*, 653, 454
- Piran, T. 2005, *Rev. Mod. Phys.*, 76, 1143
- Preece, R. D., Briggs, M. S., Mallozzi, R. S., Pendleton, G. N., Paciasas, W. S., & Band, D. L. 2000, *ApJS*, 126, 19
- Racusin, J. L. et al. 2008, *Nature*, 455, 183
- Rybicki, G. B., & Lightman, A. P. 1979, *Radiative Processes in Astrophysics* (New York: Wiley-Interscience)
- Sari, R., & Piran, T. 1997, *ApJ*, 485, 270
- Sari, R., Piran, T., & Narayan, R. 1998, *ApJ*, 497, L17
- Schlickeiser, R., & Miller, J. A. 1998, *ApJ*, 492, 352
- Silva, L. O. et al. 2003, *ApJ*, 596, L121
- Stern, B. E., & Poutanen, J. 2004, *MNRAS*, 352, L35
- Vestrand, W. T. et al. 2005, *Nature*, 435, 178
- Vurm, I., & Poutanen, J. 2009, *ApJ*, 698, 293
- Wang, X.-Y., Li, Z., Dai, Z.-G., & Mészáros, P. 2009, *ApJ*, 698, 98
- Yonetoku, D., Murakami, T., Nakamura, T., Yamazaki, R., Inoue, A. K., & Ioka, K. 2004, *ApJ*, 609, 935
- Zhang, W., MacFadyen, A. & Wang, P. 2009, *ApJ*, 692, L40
- Zhang, B., & Pe'er, A. 2009, *ApJ*, 700, L65

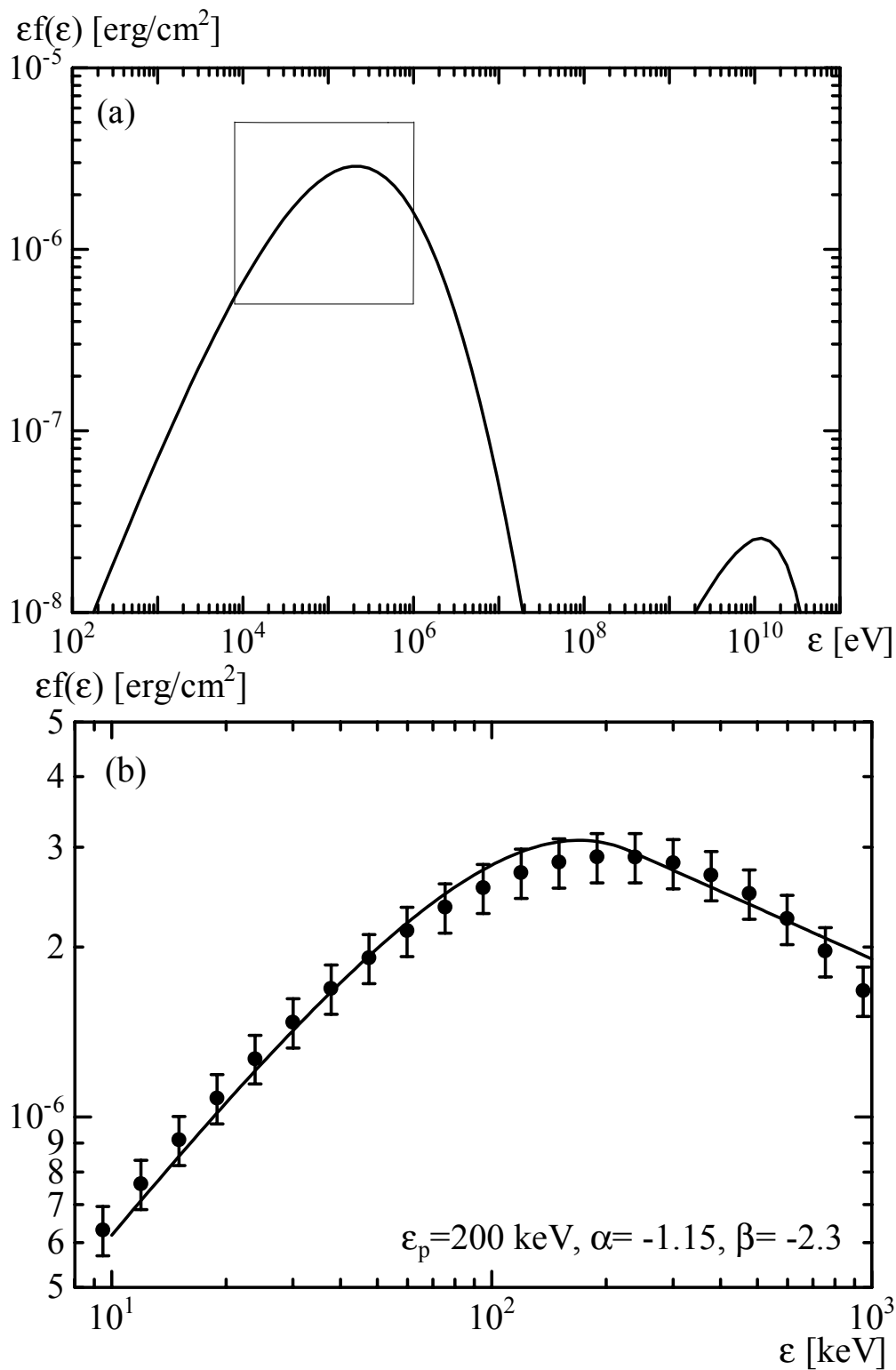


Fig. 3.— (a) Spectrum for the slow heating model with constant ξ and t_{coll} . (b) Zoom up of the upper figure (the area enclosed by the rectangle) for 10 keV – 1 MeV range. The data points are calculated spectra with 10 % error putted in by hand, and the solid line is the Band function with $\epsilon_p = 200$ keV, $\alpha = -1.15$, and $\beta = -2.3$.

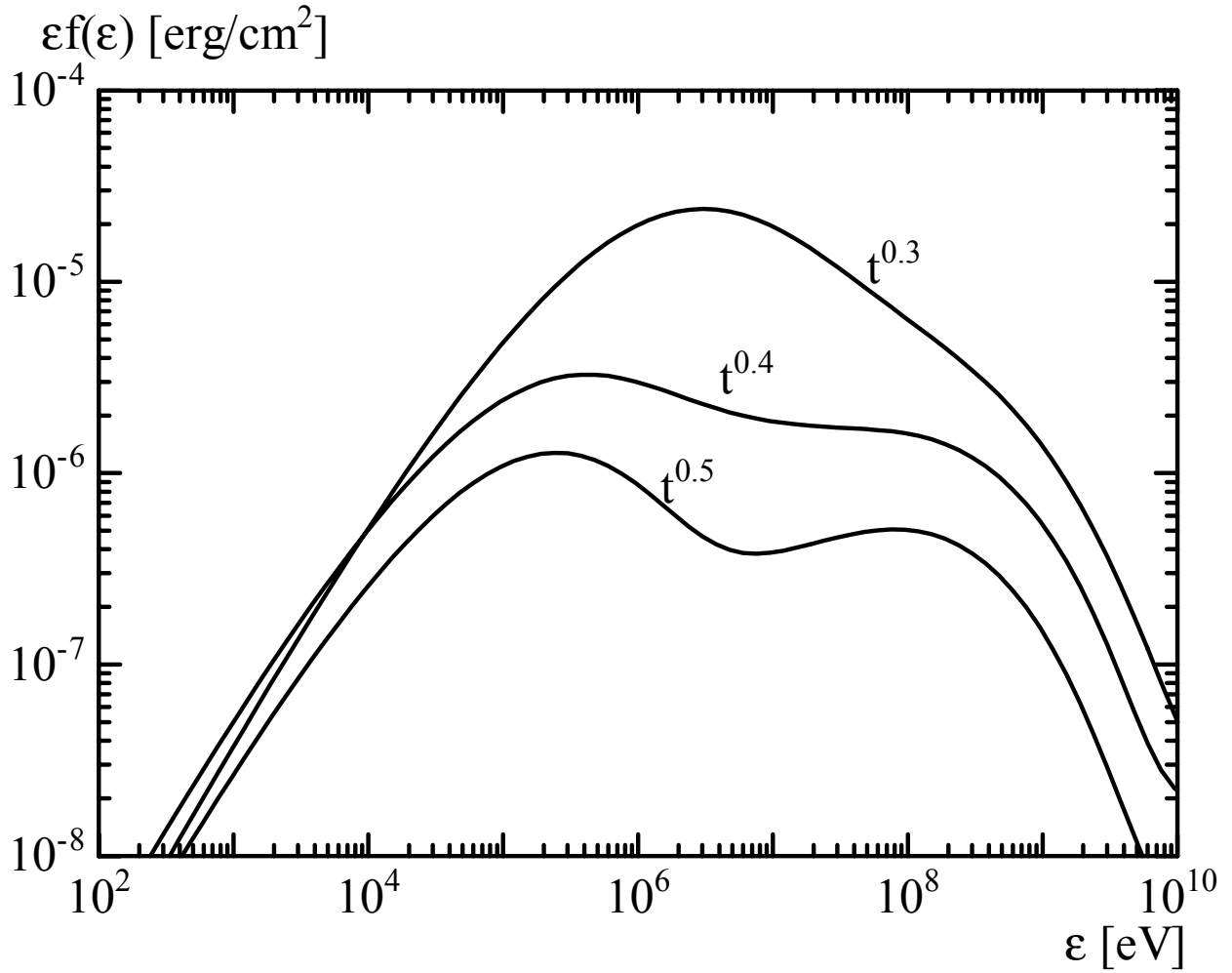


Fig. 4.— Spectra for the model of $t_{\text{coll}} \propto t^\chi$ ($D_{EE} \propto t^{-\chi}$, $\chi = 0.3, 0.4$, and 0.5), $\gamma_{\text{inj}} = 10\gamma_{\text{typ}}$, and $t_{\text{dec}} = 300t_{\text{c,typ}}$.

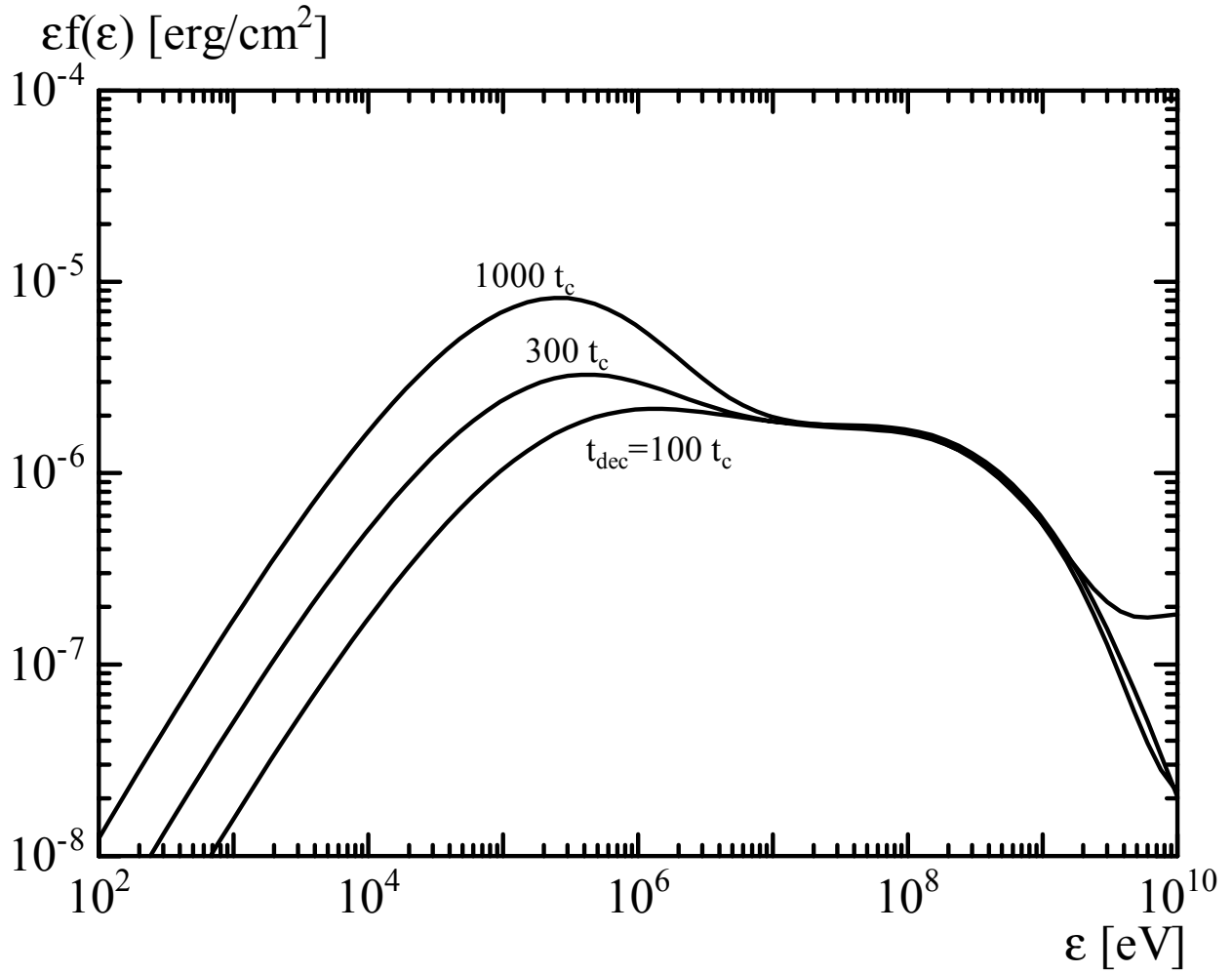


Fig. 5.— Spectra for the model of $D_{EE} \propto t^{-0.4}$, $\gamma_{\text{inj}} = 10\gamma_{\text{typ}}$, and different t_{dec} (100, 300, and $1000 t_{c,\text{typ}}$).

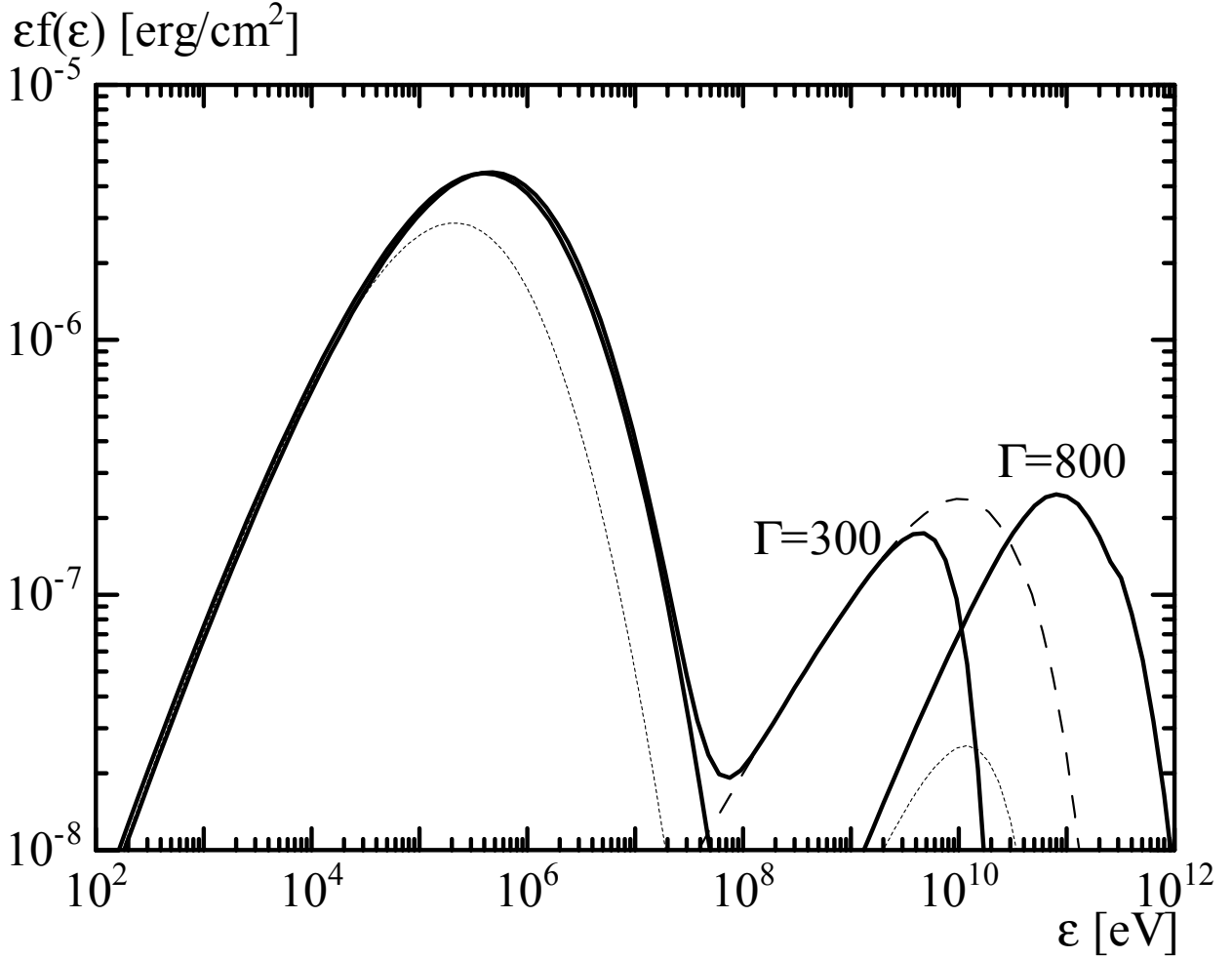


Fig. 6.— Spectra for the model of $B \propto e^{-t/t_{\text{dec}}}$, $\gamma_{\text{inj}} = \gamma_{\text{typ}}/10$, $t_{\text{dec}} = 30t_{\text{c,typ}}$ and $t_{\text{sim}} = t_{\text{dyn}}$, and different Γ (solid lines, see the text). The thin dotted line is the same as the spectrum in Figure 3, where $t_{\text{sim}} = t_{\text{dec}} \ll t_{\text{dyn}}$ and B is constant. The long dashed line is the IC component for $\Gamma = 300$ without $\gamma\gamma$ absorption effect.

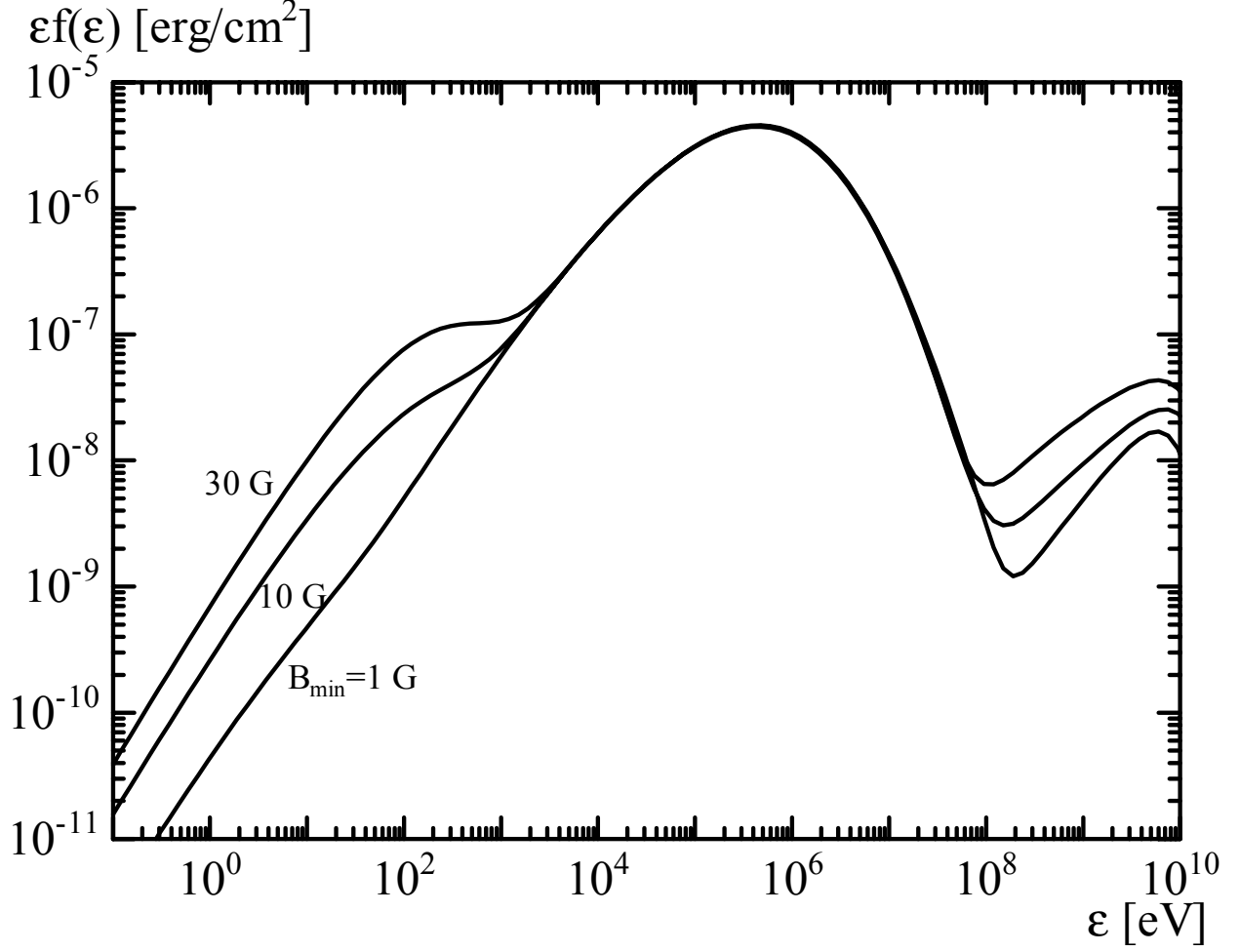


Fig. 7.— Spectra for the model of $B \propto e^{-t/t_{\text{dec}}}$, $\gamma_{\text{inj}} = \gamma_{\text{typ}}/10$, $t_{\text{dec}} = 30t_{\text{c,typ}}$ and $t_{\text{sim}} = 10t_{\text{dyn}}$, and different B_{\min} .